Performance and LDV Measurements of a Large-Scale Rotor with Synthetic Jet Actuators

Victor Maldonado[1,*] and **Soham Gupta**[2]

[1]Department of Mechanical Engineering, Texas Tech University, Lubbock, TX USA
[2]Department of Aerospace Engineering and Mechanics, University of Alabama, Tuscaloosa, AL USA
[*]corresponding author: victor.maldonado@ttu.edu

Abstract Increasing the power efficiency of rotating energy systems such as wind turbines and gas turbine rotors is critical to deriving more energy from wind or fossil fuels. In this experimental study, thrust-power and laser Doppler velocimetry measurements were made on a sub-scale three-bladed rotor containing an S809 airfoil and 20 piezoelectric-based synthetic jet actuators. The rotor was operated at rotational speeds between 250 and 1,250 revolutions per minute (RPM) and blade pitch angles of 0, 3, and 6 degrees. It was found that activating 20 synthetic jets per blade reduces the net power input to drive the rotor by up to 10.6% at a rotational speed of 500 RPM and blade pitch angle of 3 degrees. It was also shown that rotor performance parameters; figure of merit and thrust coefficient also increased by up to 28% and 9% respectively. Chordwise velocity measurements reveal that synthetic jets reduce velocity deficit within the boundary layer improving the blade sectional lift coefficient and thrust. A correlation is made between the blade tip vortex Reynolds number and spanwise velocity measurements, which indicates that the tip vortex becomes more turbulent and induces an adverse pressure gradient with increasing rotor speed and blade pitch angle. The results indicate that synthetic jets are a viable means of improving the power efficiency of a rotor with vortex Reynolds numbers under 1.8×10^5.
Keywords: unsteady aerodynamics, active flow control, synthetic jets, LDV measurements

1 Introduction

Active flow control techniques on three-dimensional, vortex-dominated rotor flows presents a fertile ground for new and innovative ways to control these flows for energy efficiency and power gains in energy systems such as wind turbines and gas turbine engines. Much of the literature on active flow control has focused on synthetic jets or plasma actuators for fixed, non-rotating blades and low Reynolds numbers flows. Synthetic jet actuators, which are the type of actuators used in the experiments of this study, are simple zero-net mass-flux devices driven by a piezo disk to ingest and expel fluid at high frequencies in a periodic manner through an orifice using only the ambient fluid with no external mass source [1][2]. The main benefits of these actuators for flow control applications are their mechanical simplicity and integration to aerodynamic bodies, as well as low power consumption.

Oster and Wygnanski [3] and Roberts [4] showed that external actuation could affect the global flow field by modifying the evolution and interaction of large-scale vortical structures. These modifications can lead to a Coanda like deflection of the separating shear layer toward the surface such that the shear-layer-amplified disturbances are advected downstream in close proximity to the surface [5]. Ultimately, this phenomenon introduces higher momentum to the separated region and in the time-averaged sense leads to flow reattachment [6]. Amitay et al. [7] and Zhang and Zhong [8] demonstrated the suppression of separation over an unconventional airfoil at moderate Reynolds numbers when the synthetic jets are activated at frequencies an order of magnitude higher than the shedding frequency of the airfoil.

The complexity of the flow physics increases drastically when the geometry of the airfoil or blade model is three-dimensional; a large spanwise flow component exists in addition to the formation of a blade tip vortex. Since blade-tip vortex shedding causes detrimental losses in aerodynamic efficiency, it is desired to minimize the size and strength or vorticity of the vortex using active flow control. More recently, active flow control has been applied near the wingtip of low aspect ratio fixed-wing model [9] with three-dimensional flow characteristics in an effort to control the behavior of primary vortex structures with secondary synthetic jet vortex structures [10]. The flow interactions of a single finite span synthetic jet near the wing tip of an unswept and swept-back wing with an aspect ratio of 4 and low Reynolds number of 100,000 were studied. For the unswept finite wing, the effect of the blowing ratio was analyzed based on three-dimensional time-averaged,

phase-averaged, and instantaneous flow fields. At low blowing ratios, spatial non-uniformities developed, due to the finite span of the jet orifice, which led to the formation of small and organized secondary structures or a streak-like pattern in the mean flow. On the other hand for high blowing ratios, turbulent vortical structures were dominant, leading to larger spanwise structures, with a larger spanwise wavelength in the mean flow. For the sweptback wing, a synthetic jet near the wing tip modifies the size and enables breakdown of the local flow structures at the location of the jet. However, due to the limited blowing ratio and presence of spanwise flow and strong wing-tip vortex, the synthetic jet was not able to influence the dominant primary flow structures to meaningfully control the flow. Greenblatt and colleagues studied the effectiveness of synthetic jet actuation as a means to control a wing-tip vortex [11][12]. They found that a small input of momentum near the tip resulted in large changes to the shear layer that rolls up into the vortex. Furthermore, the alteration of the shear layer had an effect of moving the vortex outboard. However, the surface pressures showed that the deflection of the shear layer had a small effect on the local aerodynamic loads. Other studies to control wing tip vortices using unsteady blowing [13] and plasma actuators [14] have been completed, showing an increase in vortex size and a reduction in core circulation at low angles of attack. Most recently, studies on new sweeping jet actuators show promise for flow separation control [15][16].

Experimental investigations on the application of active flow control for fully rotating blade systems have recently become an active area of research. One very recent review paper highlights studies on the application of active flow control to the low-pressure turbine section of a gas turbine to alleviate vortex shedding and separation [17]. Another study applied trailing edge and side-wall blowing to a linear stator cascade [18] in order to increase the pressure rise coefficient by 5% and significantly reduce the wake size. Other studies have also been reported on the use of active flow control technology for actual wind turbines of various power ratings. A plasma-based flow control system integrated to the surface of the blades of a 20 kW wind turbine was successfully demonstrated to improve flow stall performance and power capture [19]. Synthetic jets have also been applied in wind turbine blade models based on the S809 and S817 airfoil with simplified flow physics where the blade is not rotating but pitching. Taylor et al. [20] showed on a low Reynolds number S809 wind turbine blade that synthetic jets can reduce dynamic stall and the hysteresis involved in lift during pitching maneuvers. A reduction in hysteresis up to 73% with synthetic jets was found on a large-scale study focusing on the NREL Phase VI turbine when the blade was undergoing pitching [21]. Similar wind tunnel studies by Rice et al. [22][23] using stereo particle image velocimetry were conducted using the S817 airfoil to understand how synthetic jet vortex structures interact with primary flow structures in dynamic stall conditions. Further studies on dynamic stall have employed leading edge vortex generators, such as demonstrated experimentally by Martin et al. [24] and Mai et al. [25], and with a co-flow jet on an specially designed S809 airfoil [26].

While synthetic jets show promise in improving the aerodynamics and performance of large-scale rotating blades, the interaction between a synthetic jet and the external flow is very difficult to measure consistently at the same location using laser-based flow diagnostic techniques. The challenges are due to blade structural vibration or oscillation of the blade position as a function of rotor speed, and seeding the flow properly [27]. Nevertheless, there have been studies using laser Doppler velocimetry (LDV) to measure the unsteady flow in a low Reynolds number flow rotor [28]. The study by Maeda et al. [29] showed the feasibility of taking LDV measurements along the boundary layer of a small-scale blade inside a wind tunnel. Moreover, a series of experimental investigations have focused on measuring the rotor blade-tip vortex structures using PIV [30] and the wake using LDV by Leishman and colleagues [31][32][33]. These studies indicate the importance of understanding the nature and behavior of blade tip vortices and the wake prior to utilizing active flow control to study the interaction of multi-scale vortex structures to improve rotor performance.

1.1 Research Overview and Objectives

The present study is aimed at performing initial sets of flow and thrust measurements on a three-bladed rotor representative of a real scaled-down wind turbine rotor based on the S809 airfoil developed by the National Renewable Energy Laboratory (NREL) [34]. The main goal of the research is to determine the rotor operating conditions, e.g. rotor speeds and blade pitch angles, where active flow control with synthetic jets are able to increase rotor thrust-power efficiency. This parameter is defined as thrust generated in Newtons per unit-Watt motor power consumption. Moreover, in order to gain perspective and compare the results to other studies,

rotor performance in terms of dimensionless parameters particularly thrust coefficient and figure of merit are also presented. By measuring the mean flow along a chordwise plane with a synthetic jet near the tip of the blade with laser Doppler velocimetry, we can understand how secondary vortices from synthetic jets impact the near-wall flow and local flow reattachment to improve rotor thrust.

The active flow control technique applied utilizes piezo disk actuators to generate two-dimensional synthetic jets, and is based on the studies by the author for non-rotating and fixed-pitch wind turbine blade models [35][36]. These early experiments in a wind tunnel were performed at low Reynolds numbers between 2-4$\times 10^6$ representing quasi-laminar, two-dimensional flow where the width of the synthetic jet orifice is perpendicular to the oncoming flow direction. The current experiments were performed on a sub-scale experimental rotor at local blade flow Reynolds numbers up to approximately 1×10^6, where the flow is transitional and highly three-dimensional with varying primary turbulent length scales. Based on the LDV measurements, secondary vortices with small same-order length-scales and fixed time-scales (such as the ones produced from piezo-driven synthetic jets with fixed driving frequencies and orifice geometries) have a considerable effect in modifying the flow field very close to the location of a synthetic jet. However, viscous diffusion of small scales quickly diminishes the effect of synthetic jets downstream of the jet.

2 Experimental Methods

2.1 Rotor Test Tower

The main purpose of the rotor tower and transmission is to allow safe operation of the rotor at rotational velocities up to 1,250 revolutions per minute (RPM). The main design objective was to produce a tower system capable of generating flow Reynolds numbers up to approximately one million based on the local blade chord and free stream velocity. The tower design consists of a solid metal base with four large reinforcing flanges and leg extensions that are bolted to the floor with vibration isolation pads. The metal tower mast is removable and different mast lengths can be positioned to vary the height of the rotor hub. Experiments were performed at a rotor hub height of 3.4 m inside a high-bay test cell clear of any objects for safety and to neglect effects of the ground and ceiling on the flow and thrust measurements. Cheeseman's theory [37] was used to estimate ground effect for this study. At a dimensionless ground height, z/R = 2.82 where R is the rotor radius, the expected increase in thrust from ground effect is less than 1%.

The rotor transmission was designed to allow the rotor to operate in energy capture wind turbine mode, or as a propulsive rotor mode by mounting the rotor assembly vertically or horizontally via an aluminum adapter to the tower base. The rotor is driven in continuous locked mode (allowing reverse rotation of the motor acting as a generator in wind turbine mode) via an 8.5 kW brushless motor (model A150 manufactured by Hacker motors) with an 8 to 1 motor to rotor gear reduction. A Hall-effect sensor is integrated to the transmission drive shaft to measure the rotational speed of the rotor. The rotor head and metal swash plate enable a full range of collective and cyclic pitch control inputs to vary the blade pitch angle via four high-torque servos with an accuracy of $\pm$ 0.2 degrees. The entire rotor head and transmission system is bolted to an ATI-IA model Theta high capacity six-component load cell capable of measuring the three forces and torques with a resolution of 0.25 N and 0.0125 N-m in the rotor thrust and torque measurement respectively. The motor current is controlled with a Yep opto speed controller with a 52 Volt and 180 Amp maximum rating capable of delivering up to 9.4 kW. The power is measured with an Attopilot current sense PCB rated at 50V/ 180 Amps with input from a Matsusada model VOL50-200 high power DC supply delivering up to 10 kW. The synthetic jet power cables (8 cables from each blade) are routed from the blades to a 24-conductor high-speed slip ring mounted to the center of the rotor hub. The stationary cables from the slip ring are then routed through the ceiling and down to a signal generator and piezo amplifier (Matsusada model PZJ-0.1Px3). The electronic components are integrated to a National Instruments Labview data acquisition system (NI USB-6353 X Series) and managed through a single virtual instrument panel. The tower with experimental rotor is shown on Figure 1(a) and (b) where initial setup and testing was completed. Note this is not the location where the actual experiments of this study were conducted.

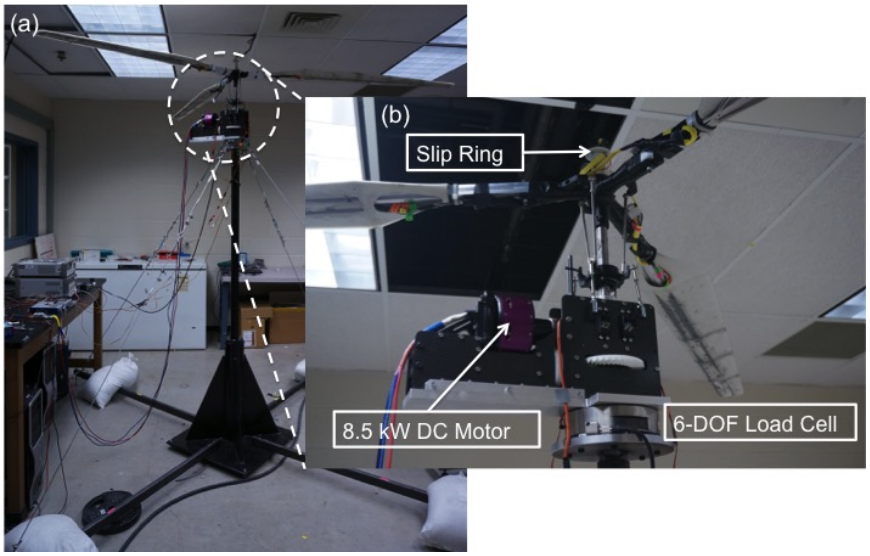

Fig. 1 (a) Rotor base and tower; (b) transmission and rotor head

2.2 Experimental Rotor

The main design objectives of the experimental rotor were to create rotor blades with the following characteristics: (1) sufficiently large to produce nominal flow Reynolds numbers of $1x10^6$ at the blade tip, (2) employ piezoelectric based synthetic jet actuators with a disk diameter of 35 mm, and (3) use the S809 airfoil and contain zero pitch twist distribution for ease in design and assembly. Computer modeling produced a rotor blade span, b of 1.06 m that tapers down from a root chord, c_r of 17.8 cm to a tip chord, c_t of 8.9 cm for a taper ratio, $\lambda = c_t/c_r$ of 0.5. The blades contain an aspect ratio of 7.79, and when the blades are mounted to the rotor hub, a rotor diameter of 2.41 m is achieved. The blades are a significantly scaled-up version of a previous blade model that was studied inside a wind tunnel by the author [38]. A unique feature is the modular design of the blades that are divided into four blade modules or sections along the span. Modular design achieves lower production cost when replacing only the affected blade section or when making improvements to the blade geometry. For the experiments in this study, the flow was measured with LDV on only the blade tip section 4. The blades are rapid prototyped using a laser-sintered process from reinforced nylon material. The blade sections are bolted to an internal aluminum spar via countersunk surface holes covered with clay for a smooth surface finish. The blade contains 20 high-performance piezo disk actuators with a diameter of 35 mm (from Omega Piezo Technologies) and rectangular synthetic jet orifices with a measurement length, l = 17.5 mm and height, h = 1.75 mm (aspect ratio of 10) placed at a local chord wise location, x/c = 0.31 from the leading edge of the airfoil. The synthetic jet velocity profile can be considered mostly two-dimensional and is oriented perpendicular to the tangential flow velocity component of the rotor. The piezo disk actuators are electronically wired together by module, such that the piezos in each module can be activated independently with a different waveform signal, frequency, and voltage amplitude.

The synthetic jets were calibrated for maximum momentum transfer using a signal generator producing a sine waveform, 3-channel piezo voltage amplifier (Matsusada PZJ-J-0.1Px3), and a Dantec Dynamics Fiber-Flow LDA system. A 60 mm optical probe and laser was centered at the synthetic jet exit plane to measure the axial velocity with a piezo driving voltage of 50 V and a wide range of input frequencies. An optimum resonant frequency, f_{res} was found that is equivalent to 1565 Hz where the piezo produced a maximum average jet velocity, u_j of 68.3 m/s. In this study, all synthetic jets inside the blades were driven at the same voltage and resonant frequency. The strength of the synthetic jet was quantified using the synthetic jet momentum coefficient. This parameter is a ratio of the momentum produced by the synthetic jets relative to the momentum of the flow over the blade, and is quantified as follows,

$$C_\mu = \frac{nI_j}{1/2\rho U_\infty^2 A_b} \tag{1}$$

where U_∞ is the local free stream velocity, A_b is the blade area, ρ is the air density, and n is the number of synthetic jets which ranges from 4 to 20 depending on the blade configuration where synthetic jets are activated. Finally, I_j is the time-average jet momentum during the outstroke, defined as,

$$I_j = \frac{1}{2}\rho A_{sj} \int_o^\tau u_j^2(t)\, dt \tag{2}$$

where τ is the synthetic jet outstroke time, A_{sj} is the area of the synthetic jet orifice, and $u_j(t)$ is the centerline velocity at the jet exit plane. The time-average jet momentum is defined only for the outstroke part of the cycle because only the outstroke imparts momentum to the flow. For a rotating rotor in stationary conditions, the freestream velocity is assumed to be equal to the product of rotational speed and local blade radius (Ωr). The inflow velocity is neglected since $\Omega r >> v_i$ and thus the airfoil angle of attack, α is assumed to be approximately equal to the blade pitch angle, θ. The synthetic jet momentum coefficient is not constant but varies according to the square of the radius (from $r = 0$ to $r = R$). The momentum coefficient is highest near the root of the blade, where Ωr approaches zero, and lowest near the tip of the blade where Ωr is a maximum. When defining the momentum coefficient for a rotating rotor, it is defined in reference to a certain module; the radius r to the center of the module and its local free stream velocity is used in the calculation. Moreover, the module planform area and number of synthetic jets contained in the module are also used. Using this definition, the range of synthetic jet momentum coefficient for the present experiments is $0.00148 \leq C_\mu \leq 0.0638$. The lowest value corresponds to operating the rotor with four jets on the blade tip section 4 at Ω = 1,250 RPM, and the highest value is obtained when activating 12 jets on blade sections 1 and 2 at Ω = 250 RPM.

The mean flow surrounding a synthetic jet were measured with a Dantec Dynamics FiberFlow LDA system and two 60 mm optical probes with 2D and 1D measurement capability in order to measure the three velocity components; *U, V, W*. The laser generator is a Dantec DopplerLite diode pumped solid state (DPSS) laser with 2 x 150 mW and 532/561 nm wavelength. The system is complete with an all-in-one processor (Burst Spectrum Analyzer, BSA F-series) configured for three velocity channels and a BSA Flow Software running on a Windows desktop for data acquisition and post-processing. A custom-built robust tower structure with motorized two-axis traversing mechanism was constructed. It was designed to place the LDV probes and laser beams angled at 30 degrees from each other and above the rotor plane angled downwards at five degrees from the rotor plane as shown on the experimental setup schematic of Figure 2. The three laser beam pairs were carefully aligned such that the measurement volume diameter was approximately 0.1 mm. Data sampling was phased-locked to the rotor speed using a trigger signal from the Hall-effect sensor with an additional time delay, such that measurements could be obtained at the predetermined rotor azimuth angle, Ψ.

Six hundred samples of instantaneous *U, V, W*, velocity data was obtained once per revolution at Ψ = 90°, and then averaged to obtain mean velocity components. Based on the layout of the laser optics with respect to the rotor blade and processing software, the uncertainty of the velocity measurements is estimated as approximately $\pm$0.35 m/s. Blade structural vibration was measured with an electronic accelerometer onboard the blade and reduced to an amplitude of $\pm$ 0.5 mm at the measurement plane by operating the rotor at speeds outside the natural excitation modes of the rotor tower. The first ten modes were computed by performing a modal analysis of the finite element model of the rotor tower. The results stress the importance of operating the rotor at speeds that exclude the following revolutions per-minute ranges to avoid excessive system vibration or damage: 440 to 480, 530 to 550, 620 to 650, and 770 to 790, and 1200 to 1230. The impact of blade vibration was fully resolved to obtain valid measurements inside the boundary layer by using real-time accelerometer data to track the vertical displacement of the blade relative to the probe measurement in order to compute the true wall-normal distance, *y'*. A fog generator (model SAFEX 10D15) was utilized to seed the flow with a mean water-based droplet size up to 1 μm. The seeding was introduced 30 cm above the rotor plane directed downward towards the measurement domain at an angle of 60 degrees from the rotor plane at high flow rates for proper flow seeding density and tracing quality. A schematic of of the experimental rotor blade with LDV measurement plane on blade section 4 (S4) near the tip of the blade is shown on Figure 3. Note the LDV measurement plane on the center of a synthetic jet orifice.

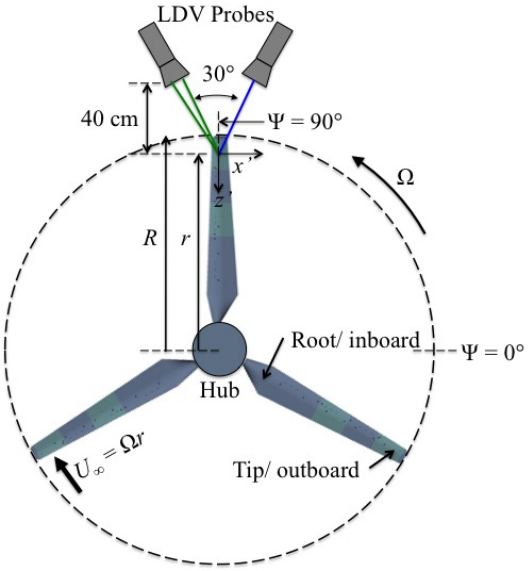

Fig. 2 Schematic of experimental setup showing the orientation of the rotor with respect to the LDV probes

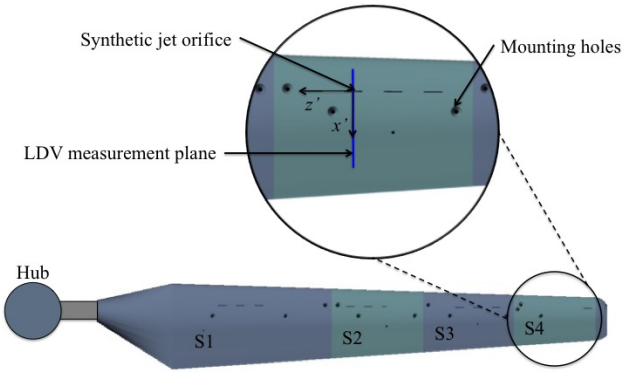

Fig. 3 Blade schematic with LDV measurement plane near the blade tip

2.3 Experimental Cases and Flow Conditions

The rotor was operated at five rotor speeds, Ω of 250, 500, 750, 1,000, and 1,250 RPM as well as three blade pitch angles, θ of 0, 3, and 6 degrees. Due to the highly unsteady nature of the blade aerodynamics, the rotor thrust and electrical power was acquired using a data sample size of 20 seconds at a sample rate of 1,000 Hz and then averaged. The uncertainty in the direct measurement of thrust from the manufacturer is within ± 0.25 N. The power reading, which is the product of current and voltage, contains a propagated uncertainty of $\pm$ 1.3% of the measurement. Finally, the blade pitch angle set by four high-torque servos is calibrated with a digital protractor prior to the experiments and contains a $\pm 0.2^{\circ}$ accuracy. Various numbers of synthetic jets were activated according to the blade configuration outlined on Table 1.

Actuation of the flow is affected at frequencies that are of the same order of magnitude $F+ \sim O(1)$ as the characteristic shedding frequency. More precisely, the ratio between the synthetic resonant frequency (f_{res} = 1565 Hz) to the characteristic shedding frequency ($f_{char} = U_{\infty}/c$) of the airfoil is in the range of $1.05 \leq f_{res}/f_{char} \leq 5.24$ at the measurement location for all rotor speeds tested. This type of flow control technique produces the formation of vortical structures at the resonant frequency, and time-periodic vorticity flux and flow reattachment [39]. The local flow Reynolds number at the LDV measurement plane is calculated according to $Re = U_{\infty}c/\nu$, where c is the local airfoil chord and ν is the air kinematic viscosity. The local Reynolds and Mach numbers for each rotor operating speed are given on Table 2.

Six hundred instantaneous measurements of *U, V, W* velocity components were acquired and time-averaged

Table 1 Experimental blade flow parameters

Configuration	Synthetic Jet Actuation	Number of Jets
A	Baseline: no synthetic jet actuation	0
B	All blade sections (1, 2, 3, 4)	20
C	Blade section 4 (blade tip)	4
D	Blade section 1 and 2	12
E	Blade section 3 and 4	8

Table 2 Flow Reynolds and Mach number at the blade measurement plane

Ω (RPM)	Re_∞	M_∞
250	2.02x10^5	0.089
500	4.04x10^5	0.18
750	6.06x10^5	0.27
1,000	8.08x10^5	0.36
1,250	1.01x10^6	0.45

in order to obtain mean velocity profiles. For this investigation, one measurement plane was selected across the center of the third synthetic jet from the blade tip at z' = 0 mm as shown on Figure 3. The LDV probes were traversed to obtain data at four locations upstream and downstream of the synthetic jet along -8.75 mm $\leq x' \leq$ 26.25 mm, and wall-normal data along 0 mm $\leq y' \leq$ 5.25 mm. Zero corresponds to the wall at the local measurement location, and the measurement resolution is equal to *h/4* = 0.438 mm. The measurement coordinates are non-dimensionalized with synthetic jet orifice height, and thus the flow is plotted along coordinates $-5 \leq x'/h \leq 15$ and $0 \leq y'/h \leq 3$. LDV data was obtained for rotor speeds of Ω = 250, 750, and 1,250 RPM at blade pitch angles of $\theta = 0^\circ$, 3°, and 6°.

3 Results

3.1 Rotor Performance Measurements

The thrust-power performance of the rotor was quantified for the baseline without flow control and different combinations of synthetic jet forcing on the blades as indicated on Table 1. The main objective here is to show that synthetic jets are a viable means of increasing the thrust-power performance of a rotor, as defined by thrust-to-power consumption and figure of merit. The electrical input power as a function of rotor thrust is presented in Figures 4(a, b, and c) for blade pitch angles, $\theta = 0^\circ$, 3°, and 6° respectively. The thrust and power measurements are a result of the integrated sectional lift and drag properties of the blade and various non-ideal flow and mechanical losses of the system. In Figure 4(a) for $\theta = 0^\circ$, it is visible that activating the blade with different combinations of synthetic jets yields a lower power consumption for a given thrust compared to the baseline. Activating all 20 synthetic jets on blade sections 1 through 4 produces the best performance, however it is evident by the results that focusing jet actuation on the two outboard blade sections 3 and 4 with eight jets is very nearly as effective. This behavior repeats itself for $\theta = 3^\circ$ and $\theta = 6^\circ$, only this time much higher thrust is produced due to normal operating conditions which places the blade sections at moderate angles of attack and lift coefficient values. It is hypothesized that synthetic jet actuation near the blade tip is more effective in increasing thrust-power efficiency compared to the blade root due to higher disk loading (thrust produced per unit blade area) near the tip. This makes any flow reattachment from flow control more sensitive to increasing sectional lift and decreasing pressure drag due to flow separation, thereby having a larger impact on rotor thrust and power.

In order to closely examine rotor performance for all flow control (FC) cases, the rotor thrust generated divided by input electrical power to drive the rotor (T/P) efficiency as a percentage over the baseline (BL) is

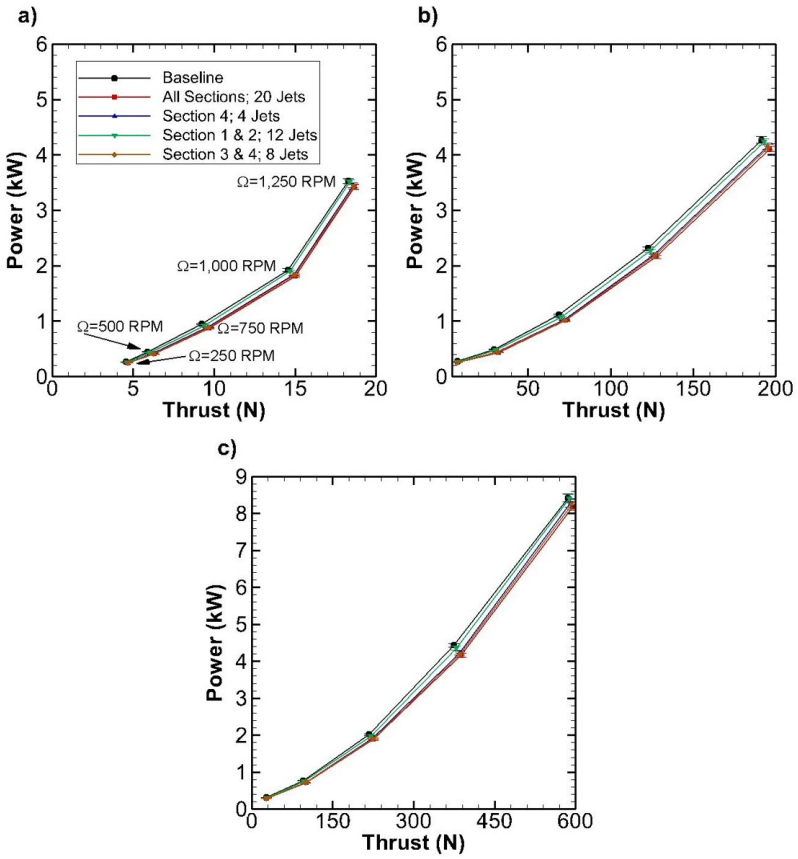

Fig. 4 Rotor power as a function of thrust for the baseline and flow control cases at blade pitch angles: a) θ = 0°, b) θ = 3°, and c) θ 6°

plotted on Figure 5(a, b, and c) for θ = 0°, 3°, and 6° respectively and is defined as follows,

$$\eta_{T/P} = \frac{(T/P)_{FC} - (T/P)_{BL}}{(T/P)_{BL}} * 100 \tag{3}$$

It is clearly apparent that flow control with synthetic jets is effective in considerably increasing thrust-power efficiency, and is highly dependent on rotor speed, blade pitch angle, and blade location where the synthetic jets are activated. In terms of location, maximum performance per synthetic jet is achieved by activating four synthetic jets on the blade tip on section 4. The synthetic jets on the inboard region of the blade in section 1 and 2 are low-performance in comparison. Moreover the results are non-linear; the efficiency of activating jets on sections 1 & 2 and 3 & 4 separately sums to a larger value than the efficiency when all 20 jets are utilized at once. This suggests that there are adverse flow interactions between neighboring synthetic jets in a three-dimensional flow field that cause diminishing returns when activating a large number of jets on the blade.

For each blade configuration, the thrust-power efficiency reaches a local maximum value at a rotor speed, Ω = 500 RPM, then sharply decreases as a function of speed up to 1,250 RPM. As the efficiency decreases, the freestream velocity and flow momentum over the blade increases, thereby significantly reducing the relative momentum transfer of the synthetic jets and their ability to suppress flow separation. A similar behavior was measured by the author for a fixed non-rotating wind turbine blade model inside a wind tunnel as the Reynolds number was increased [36]. The results suggest that for high rotor speeds and/or local flow Reynolds numbers beyond $1x10^6$ representative of industrial-scale wind turbines or gas turbines, more powerful synthetic jet actuators are needed. The increased energy capture or thrust-power efficiency must outweigh the manufacturing complexity and added cost of incorporating synthetic jet actuators. In terms of the power input required to drive

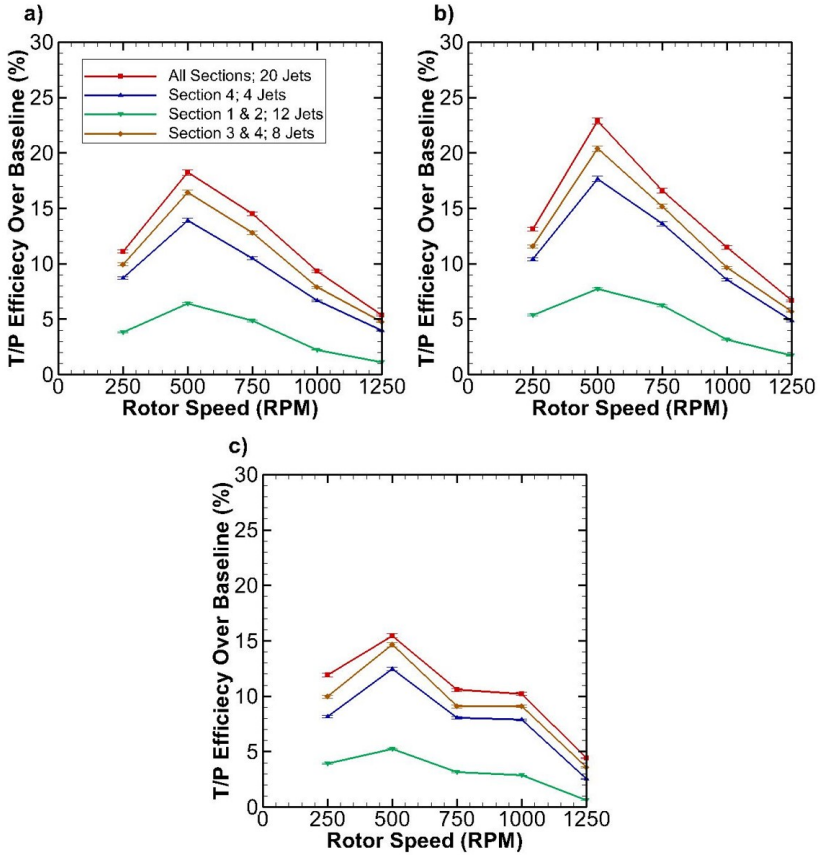

Fig. 5 Rotor thrust-power efficiency over the baseline as a function of rotor speed for flow control cases at blade pitch angles: a) $\theta = 0°$, b) $\theta = 3°$, and c) θ 6°

the piezo disk actuators relative to the power savings to drive the rotor, there is a net reduction in the overall input power to the system. In this study each piezo was measured to consume an average of 0.185 W at an input voltage of 50 V, generating a synthetic jet with an average orifice exit velocity of 68.3 m/s. Activating a total of 60 synthetic jets for the three-bladed rotor requires 11.1 W of power. If we consider the best performing case on Figure 5(b) when activating all jets for $\theta = 3°$ and $\Omega = 500$ RPM with a thrust-power efficiency of 22.9% over the baseline, we find that the input power is 0.436 kW compared to the baseline for the same conditions of 0.492 kW. This amounts to a net power savings of approximately 44.9 W, which is 9.1% of the original baseline power. This surprisingly favorable result serves as a motivation to study and advance active flow control techniques, specifically those based on synthetic jets, for large-scale rotor applications.

To further understand the significance of the flow control approach presented, the rotor figure of merit, *FM* as a function of thrust coefficient, C_T are presented on Figure 6. The *FM* is a dimensionless parameter of rotor power efficiency that compares the ideal power relative to actual power required to produce thrust,

$$FM = \frac{P_{ideal}}{P_{actual}} = \frac{\frac{T^{3/2}}{\sqrt{2\rho A}}}{P_{elec}} \tag{4}$$

where ideal power is based on momentum theory and contains the air density, ρ and rotor disk area, A. The actual power is the input power required to produce thrust, T which in this case is the electrical power supplied to the motor to drive the rotor. The thrust coefficient is also a dimensionless performance parameter that indicates the potential of a rotor to generate thrust relative to its disk area and blade tip velocity (ΩR),

$$C_T = \frac{T}{\rho A \Omega^2 R^2} \tag{5}$$

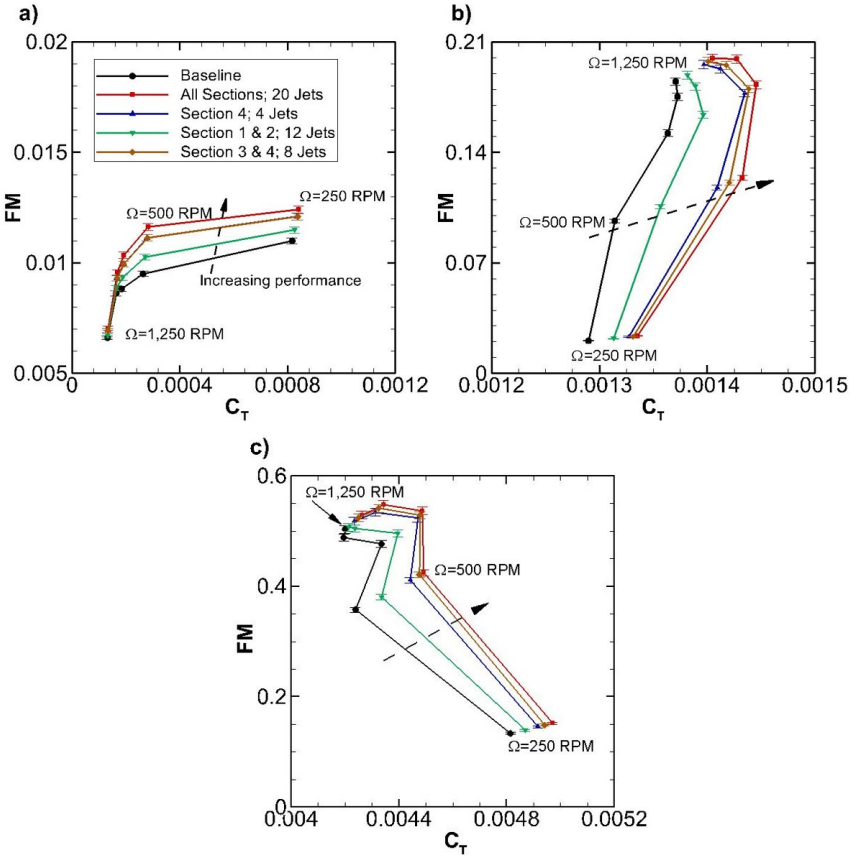

Fig. 6 Rotor figure of merit as a function of thrust coefficient for the baseline and flow control cases at blade pitch angles: a) $\theta = 0^\circ$, b) $\theta = 3^\circ$, and c) θ 6°

With normal favorable operating conditions at $\theta = 3^\circ$ and 6° in Figures 6(b) and (c) we observe markedly different results. The *FM* increases significantly to expected values at high rotational velocities while the C_T reverses trend from a minimal increase at $\theta = 3^\circ$ to a decrease at $\theta = 6^\circ$. Note the very small x-axis range in C_T. This effect is attributed to larger increases to the induced and profile power of the rotor at higher angles of attack and thrust [40]. The best flow control performance, as discussed in the thrust-power results, occurs at rotor conditions of $\theta = 3^\circ$ and Ω = 500 RPM. The arrow in the plots gives the direction of increasing performance from the baseline both in terms of *FM* and C_T for all flow control cases. Again, the blade configuration involving 20 synthetic jets achieves the largest gain in performance; a 28% and 9% gain in *FM* and C_T respectively. Figure 6(c) at $\theta = 6^\circ$ shows maximum *FM* is produced at Ω = 1,000 RPM reaching a value of *FM* = 0.55 when actuating all jets, compared to *FM* = 0.49 for the baseline at the same rotor speed. This represents a considerable increase in power efficiency of 12%.

3.2 Chordwise Velocity Distributions

The flow over the blade airfoil was measured and time-averaged at four chord-wise measurement locations; *x/c* = 0.219 (M1), 0.309 (M2), 0.400 (M3), and 0.581 (M4) for the baseline and flow control case for blade section 4 only. Measurement M2 coincides with the location of the synthetic jet. Moreover, relative to the synthetic jet at *x/h* = 0, M1 is located 5 orifice heights (5*h*) upstream of the synthetic jet at *x/h* = -5, M3 is 5*h* downstream at *x/h* = 5, and M4 is 15*h* downstream at *x/h* = 15. The turbulence intensity, T_u inside of the boundary layer was calculated from the instantaneous LDV measurements. It was found that T_u varies widely from $2.3\% \leq T_u \leq 18.6\%$, and generally increases with rotor speed, blade pitch angle, chordwise distance, and depth into the boundary layer. A turbulence intensity above 10% was found at Ω = 1,000 RPM and 1,250 RPM

for $\theta = 3^\circ$ and 6°, where the local Re_∞ is $8.08\text{x}10^5$ and $1.01\text{x}10^6$. The boundary layer under these conditions is predominantly a turbulent boundary layer.

Figure 7 presents the nondimensional chordwise velocity component, U/U_∞ for M1 through M4 and θ = 0°, 3°, and 6° for the baseline and flow control case with $C_\mu = 0.0371$ at a rotor speed, $\Omega = 250$ RPM. This corresponds to a Reynolds number of $2.02\text{x}10^5$ at the blade measurement locations. Note that for the calculation of C_μ, only the area of the blade section 4 was considered, and the freestream velocity (Ωr) value of 29.88 m/s is evaluated at the synthetic jet with a spanwise location, $r/R = 0.947$. Figures 7(a, e, and i) show that upstream of the synthetic jet there is no effect on the flow. The boundary layer develops over the surface of the blade and grows from a thickness, δ of approximately $0.5h$ (0.88 mm) at M1 to $0.8h$ at M4 for $\theta = 0^\circ$ at $U/U_\infty \cong 1$. We can clearly see the effect of flow control in the boundary layer, which is to reduce flow velocity deficit and momentum loss. Moreover, synthetic jets also influence the outer flow by increasing momentum particularly at the location of the jet on M2 and generally diminishes further downstream. The velocity distributions seem to converge at a wall-normal distance approaching $y'/h = 3$, indicating that synthetic jets are most effective at modifying chordwise velocity near the wall.

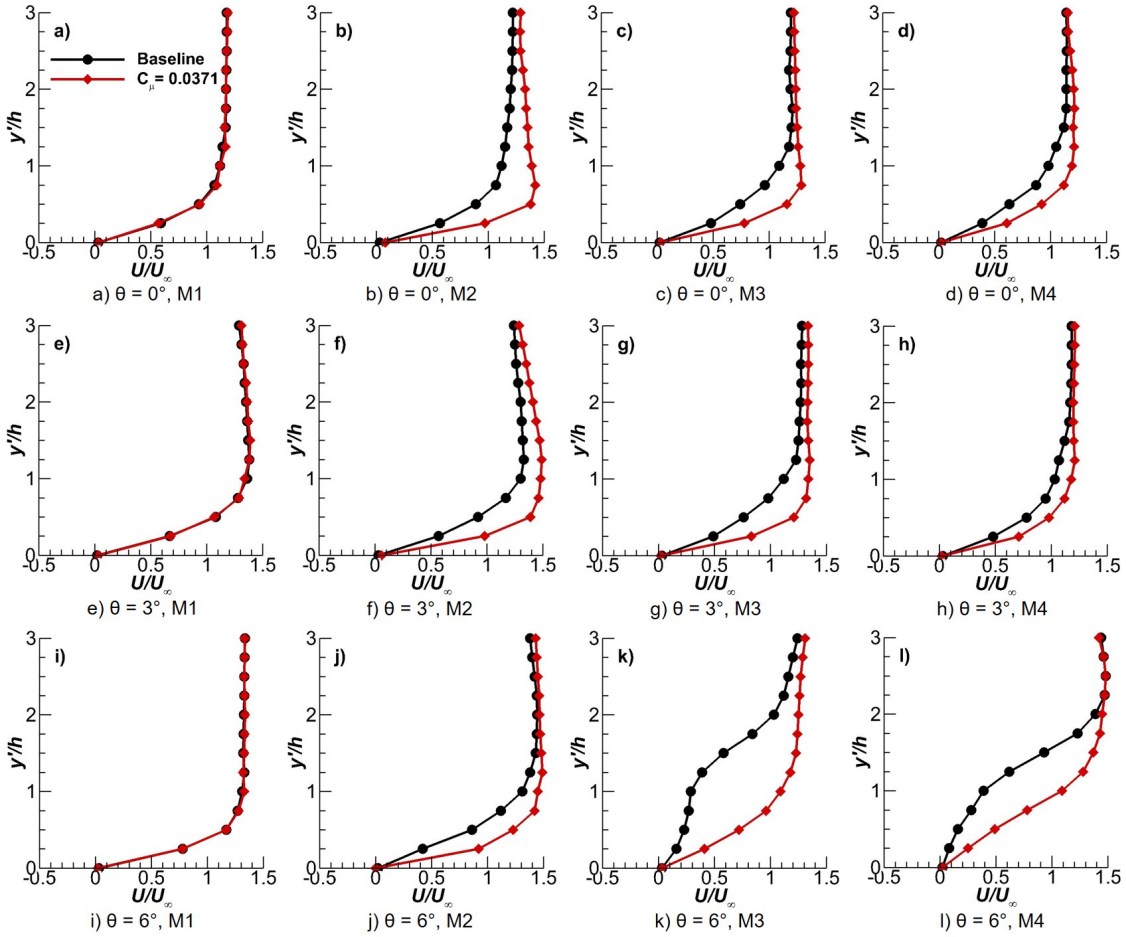

Fig. 7 Distribution of normalized chordwise velocity, U/U_∞ for the baseline flow and when blade section 4 jets were activated with $C_\mu = 0.0371$ at $\Omega = 250$ RPM

As the blade pitch angle is increased to $\theta = 6^\circ$ in Figure 7(k and l) for the baseline case, there is an inflection point in the velocity profile which indicates the presence of an inviscid instability. Moreover, a reduction of the profile wall slope, $\partial U/\partial y'$ and boundary layer momentum suggests that flow separation is imminent. Flow control is shown to be able to restore some flow momentum in the boundary layer and consequently enhance lift compared to the baseline.

In the next set of velocity distributions on Figure 8, the rotor speed was increased to 750 RPM while maintaining the same synthetic jet orifice exit velocity. This effectively increases the free stream velocity and

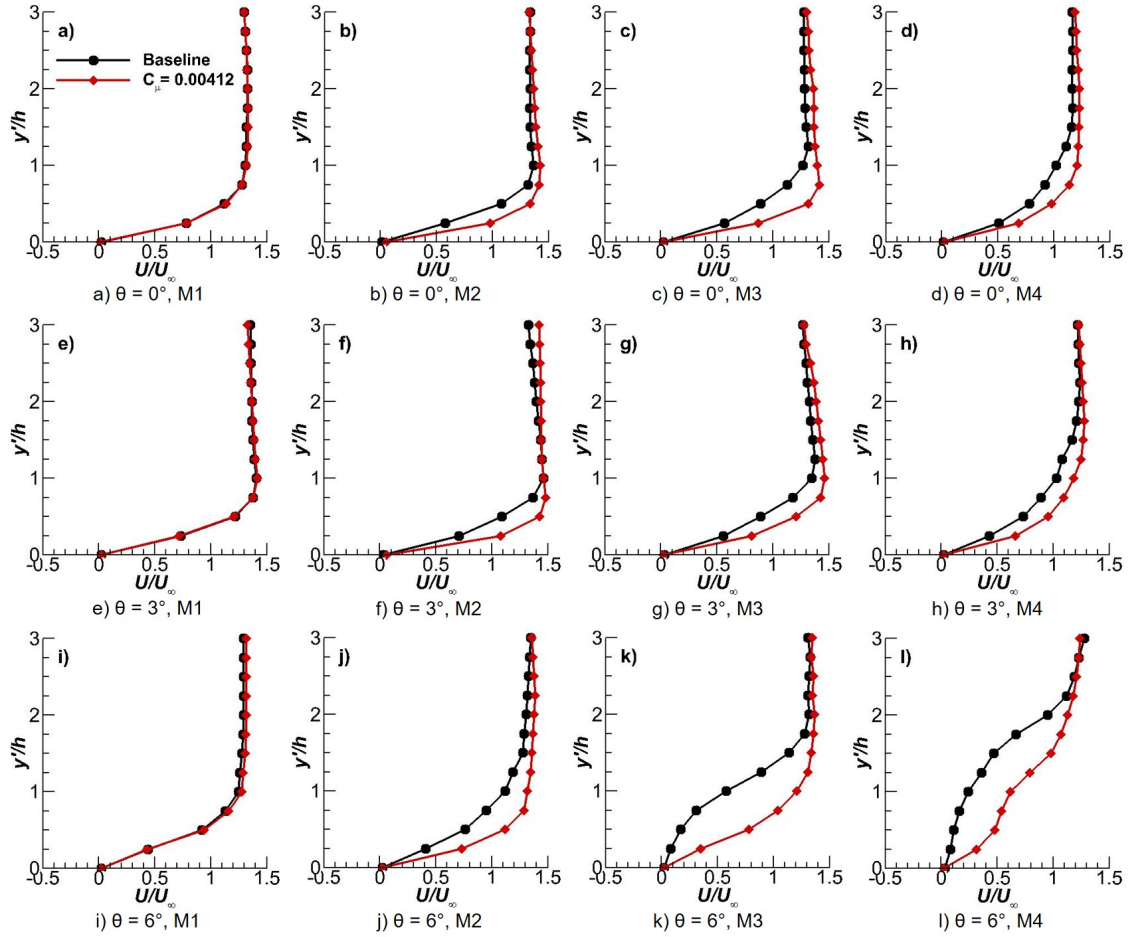

Fig. 8 Distribution of normalized chordwise velocity, U/U_∞ for the baseline flow and when blade section 4 jets were activated with C_μ = 0.00412 at Ω = 750 RPM

reduces the synthetic jet momentum coefficient to C_μ = 0.00412. Flow control is less able to energize the boundary layer and reduce the velocity deficit at lower synthetic jet momentum coefficients. In the case when the flow is on the verge of separation such as in Figure 8(k and l), synthetic jets are again able to provide momentum and delay separation.

As the rotor speed is increased further to Ω = 1,250 RPM in Figure 9, the local Reynolds number reaches 1.01x10^6 and the boundary layer transitions to turbulent flow. There is a noticeable reduction in the initial boundary layer thickness. In the favorable pressure region of the airfoil at M1 or x'/h = -5 for $\theta = 0^\circ$ in Figure 9(a), the boundary layer thickness reaches a height of $y'/h \simeq 0.25$ or $\delta \simeq 0.48$ mm. For the previous cases at Ω = 750 and 250 RPM respectively, the boundary layer at M1 is $\delta \simeq 0.66$ mm and $\delta \cong 0.97$ mm. However, the rate of boundary layer growth at Ω = 1,250 RPM is higher with chordwise distance and blade pitch angle. This is characteristic of a turbulent boundary layer with high levels of turbulence intensity, where T_u up to $\simeq$ 18.6% was measured for Ω = 1,250 RPM at $\theta = 6^\circ$ and M4 (x/c= 0.581). It is unclear how much effect the blade tip vortex has on boundary layer growth and turbulence intensity. There is evidence of a role in promoting boundary layer separation and slight reverse flow as shown for $\theta = 6^\circ$ and M4 in Figure 9(l), whereas this does not occur at lower rotor speeds and blade pitch angles. Finally, it is very important to note that even though the effect of the synthetic jet is diminutive for Ω = 1,250 RPM at this particular blade measurement location, actuation of blade section 4 with three other synthetic jets manages to increase thrust-power efficiency between 2-5% as indicated in Figure 5.

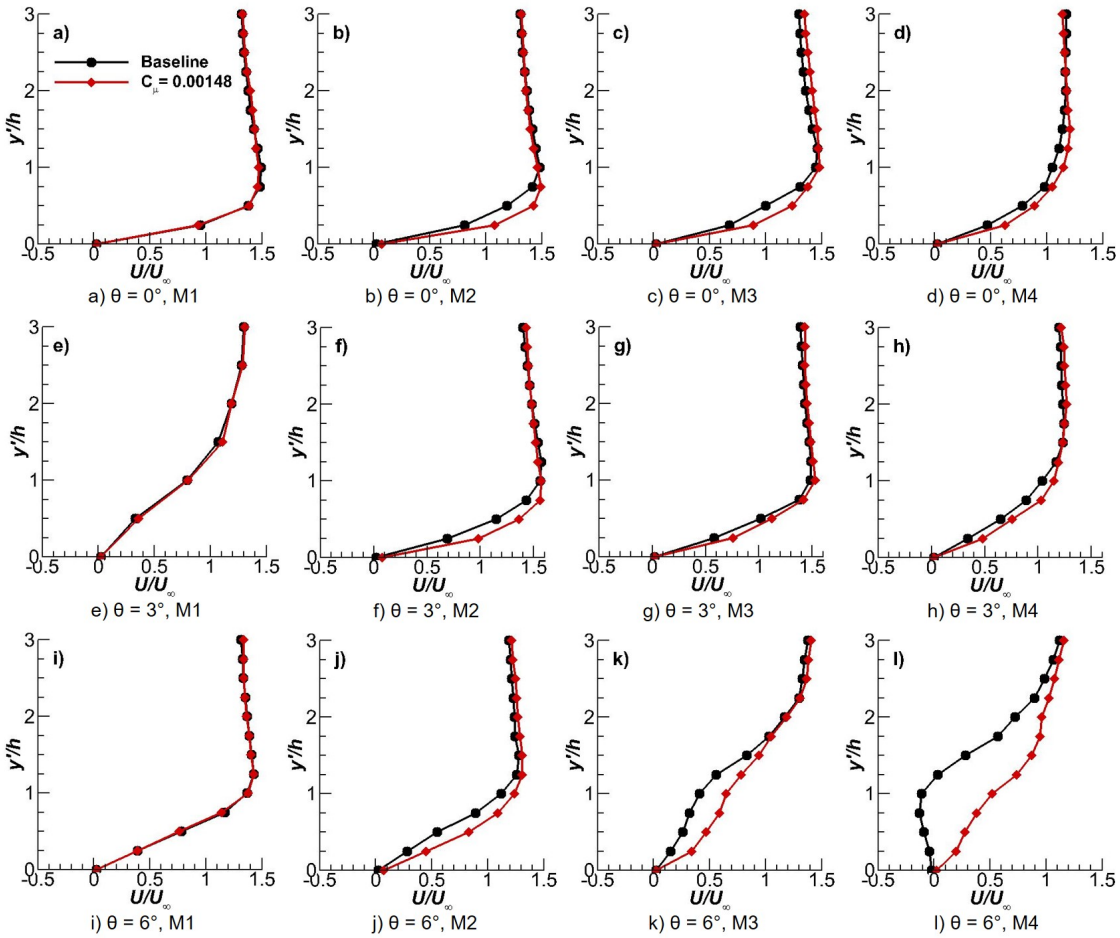

Fig. 9 Distribution of normalized chordwise velocity, U/U_∞ for the baseline flow and when blade section 4 jets were activated with C_μ = 0.00148 at Ω = 1,250 RPM

3.3 Spanwise Velocity Distributions

The spanwise velocity component significantly contributes to three-dimensional flow encountered in the rotor and must be measured in order to properly characterize the flow. Figure 10 presents the nondimensional spanwise velocity component, W/U_∞ at the four measurement locations, M1 to M4 for blade pitch angles θ = 0°, 3°, and 6° at a rotor speed Ω = 750 RPM.

We can observe that within the boundary layer very close to the wall, the flow travels outboard towards the blade tip. Subsequently it encounters a blade tip vortex structure that induces flow in the inboard direction thereby diminishing its velocity outside the boundary layer. Moreover, as the flow travels along the airfoil from leading edge to trailing edge in a skewed manner due to spanwise velocity, it turns towards the blade tip at a faster rate due to an increase in the maximum negative spanwise velocity from M1 to M4 in Figure 10(a-d), 10(e-h), and 10(i-l) respectively for θ = 0°, 3°, and 6°. It is also evident that the blade-tip vortex becomes much stronger at higher blade pitch angles, for example at θ = 6° in Figure 10(i-l). The velocity distribution away from the wall becomes highly skewed towards positive W/U_∞, indicating that the tip vortex is inducing higher positive spanwise flow that opposes the spanwise component of freestream velocity. Flow control has a noticeable but very minor effect in modifying the baseline flow induced by the blade tip vortex above y'/h = 1.

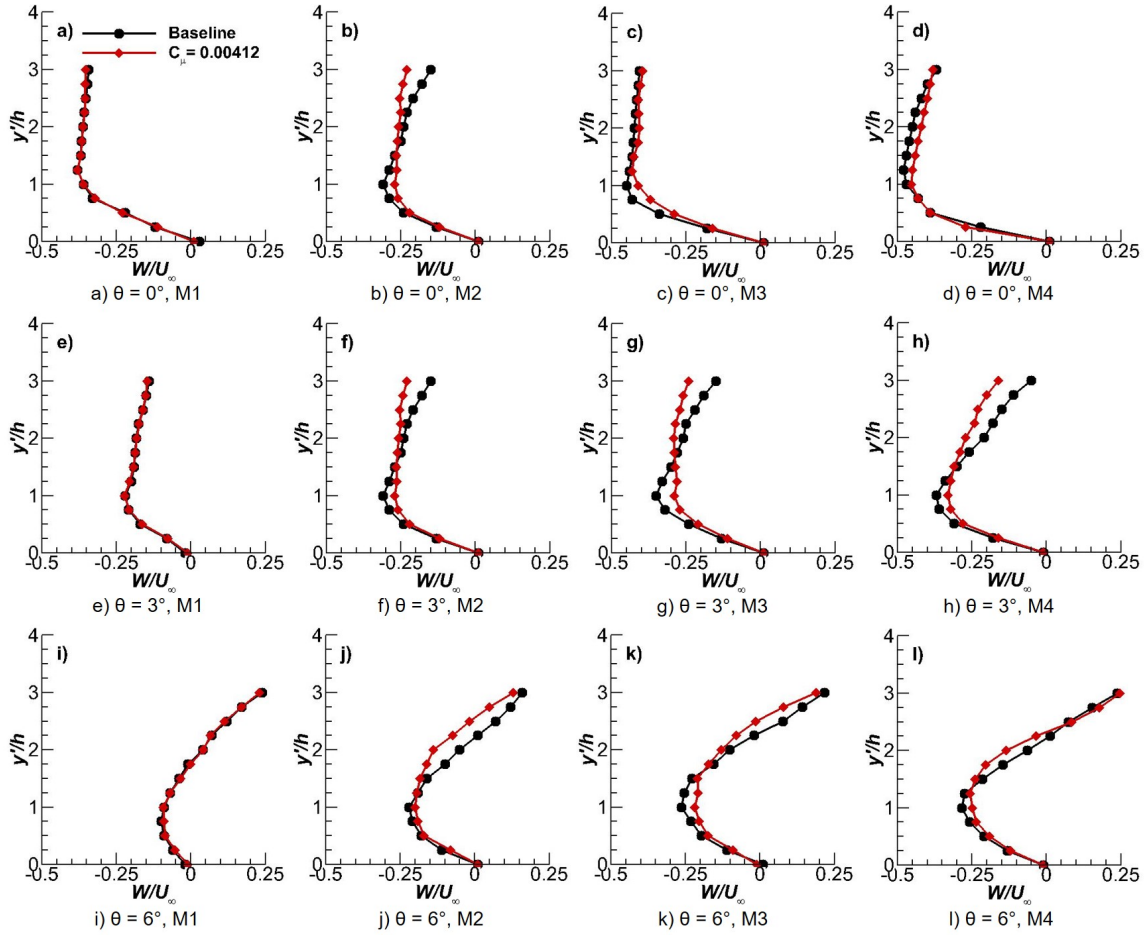

Fig. 10 Distribution of normalized spanwise velocity, W/U_∞ for the baseline flow and when blade section 4 jets were activated with $C_\mu = 0.00412$ at $\Omega = 750$ RPM

3.4 Vortex Reynolds Number

The turbulent nature and length scales of the blade tip vortex can be described using the vortex Reynolds number [40] as follows,

$$Re_V = \frac{\Gamma_v}{\nu} = \frac{2(\Omega R)R}{\nu AR}\left(\frac{C_T}{\sigma}\right) \tag{6}$$

where Γ_v is the circulation of the tip vortex which is directly related to lift production, and ν is the kinematic viscosity of air at standard conditions. The expression is simplified to defining the vortex Reynolds number in terms of the rotor thrust coefficient, C_T, blade solidity, σ and rotor blade geometric and operating parameters; aspect ratio, AR and tip speed, ΩR which were directly calculated during rotor testing. The Re_v allows a scaling analysis given by Iversen [41] to be done between model rotors and a full-scale rotor, thereby estimating the effect of the proposed flow control technique on real-world thermo-fluid systems.

The calculation of Re_v as a function of C_T and θ for the baseline (BL) and synthetic jet activation in all blade sections (FC S1-S4) and just section 4 (FC S4) are presented on Figure 11.

The magnitude of vortex Reynolds number is strongly dependent on blade pitch angle, and the enormous difference in magnitude between Re_v at $\theta = 0°$ and $\theta = 6°$ can be appreciated in the same plot. For $\theta = 0°$ when blade thrust loading is very low and consequently Re_v ranges between [4.2 – 6.5] x10^3, there exists a relatively weak blade tip vortex characterized as transitional flow outside the vortex core according to Iversen. At $\theta = 3°$ and 6° the vortex Reynolds numbers reach values between [1 – 5.4] x10^4 and [3.7 –16.3] x10^4 respectively, and

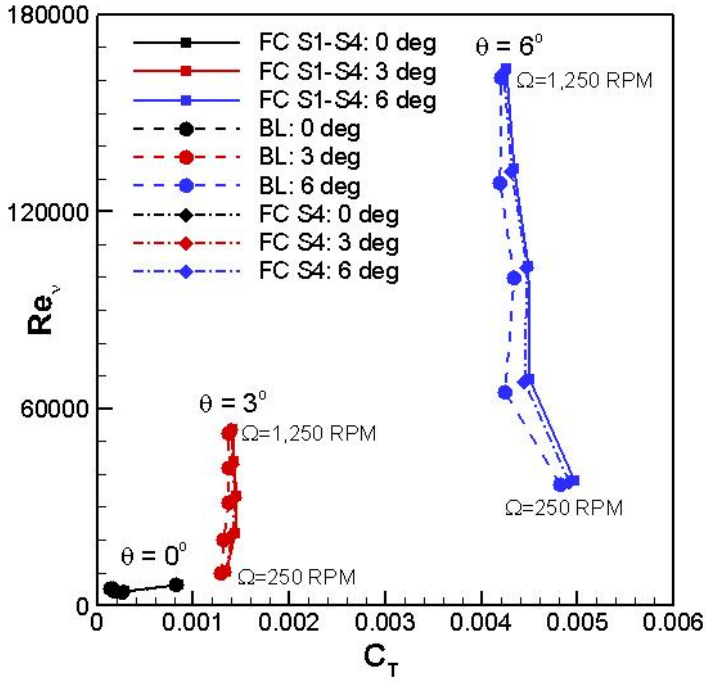

Fig. 11 Vortex Reynolds number as a function of thrust coefficient at $\theta = 0°$, 3°, and 6°

the tip vortex is categorized as turbulent. In the set of results at $\theta = 3°$ and more significantly at $\theta = 6°$, we can observe that flow control increases vortex Reynolds number due to higher thrust coefficients measured earlier. Moreover as Re_v increases, the vortex core grows with higher induced velocities and turbulent length scales. The impact of larger vortex size and induced velocity is readily observed on the spanwise velocity distributions of Figures 9(i-l) as explained earlier.

4 Conclusions

Experiments on a sub-scale rotor with synthetic jets were conducted and show that a considerable increase in thrust-power efficiency is possible at rotor speeds where synthetic jets can impart sufficient momentum to the boundary layer relative to the baseline flow over the blade. This was most pronounced at rotational velocities of $\Omega = 500$ and 750 RPM. At $\Omega = 250$ RPM where the synthetic jet momentum coefficient for the entire blade is highest, it is believed based on the study by Vasile [9] that synthetic jets near the blade root on sections 1 and 2 actually cause local flow separation in regions where the ratio of jet to freestream velocity is approximately two or more. It is therefore desirable to lower the synthetic jet velocity in the inboard region of the blade at low rotor speeds to improve performance. It was also shown that for the amount of synthetic jets activated, control of the flow in the blade tip region holds the largest gains in improving the thrust-power efficiency of the blade.

The blade tip vortex is a critical factor which strongly influences the fluid dynamics of the blade tip by inducing positive spanwise flow and adverse pressure gradient as the rotor speed and blade pitch angle increase. Moreover the magnitude of these effects was linked to the vortex Reynolds number, which is an indication of vortex size and inertial strength. In conclusion, flow control using synthetic jets can improve the aerodynamics and performance of a rotor. The technique presented seems to be scalable to larger rotors, however system factors such as reliability of the actuators in real operating conditions must be evaluated before it can be implemented in actual rotor-based energy or propulsion systems.

References

[1] Glezer A, Amitay M (2002) Synthetic jets. *Annual Review of Fluid Mechanics*, vol. 34, pp 503-529. doi: 10.1146/annurev.fluid.34.090501.094913.

[2] Cattafesta L, Sheplak M (2011) Actuators for active flow control. *Annual Review of Fluid Mechanics*, vol. 43, pp 247-272. doi: 10.1146/annurev-fluid-122109-160634.

[3] Oster D, Wygnanski I J (1982) The forced mixing layer between parallel streams. *Journal of Fluid Mechanics*, vol. 123, pp 91-130. doi: 10.1017/S0022112082002973.

[4] Roberts F A (1985) Effects of periodic disturbances on structure of mixing in turbulent shear layers and wakes. PhD Thesis, California Institute of Technology, Pasadena, CA.

[5] Seifert A, Bachar T, Koss D, Shepshelovich M, Wygnanski I J (1993) Oscillatory blowing: a tool to delay boundary-layer separation. *AIAA Journal*, vol. 31, pp 2052-2060. doi: 10.2514/3.49121.

[6] Post M, Corke T (2006) Separation control using plasma actuators: dynamic stall vortex control on oscillating airfoil. *AIAA Journal*, vol. 44, pp 3125-3135. doi: 10.2514/1.22716.

[7] Amitay A, Smith D R, Kibens V, Parekh D E, Glezer A (2001) Modification of the aerodynamics characteristics of an unconventional airfoil using synthetic jet actuators. *AIAA Journal*, vol. 39, pp 361-370. doi: 10.2514/2.1323.

[8] Zhang S, Zhong S (2010) An experimental investigation of flow separation control using an array of synthetic jets. *AIAA Journal*, vol. 48, pp 611-623. doi: 10.2514/1.43673.

[9] Vasile J D, Amitay M (2015) Interaction of a finite-span synthetic jet near the tip of a sweptback wing. *Physics of Fluids*, vol. 27, no 067102-27. doi: 10.1063/1.4921844.

[10] Lawson J M, Dawson J R (2013) The formation of turbulent vortex rings by synthetic jets. *Physics of Fluids*, vol. 25, no 105113. doi: 10.1063/1.4825283.

[11] Greenblatt D (2012) Fluidic control of a wing tip vortex. *AIAA Journal*, vol. 50, pp 375-386. doi: 10.2514/1.J051123.

[12] Vey S, Nayeri C N, Paschereit C O, Greenblatt D (2010) Leading edge and wing tip flow control on low aspect ratio wings. In: Proceedings of the 40th Fluid Dynamics Conference and Exhibit, AIAA 2010-4865. doi: 10.2514/6.2010-4865.

[13] Simpson R G, Ahmed N A, Archer R D (2002) Near field study of vortex attenuation using wing tip blowing. *Aeronautical Journal*, vol. 102, pp 117-200. doi: 10.1017/S0001924000012847.

[14] Chappell S, Angland D (2012) Active control of a wing tip vortex with a dielectric barrier discharge plasma actuator. In: Proceedings of the 6th AIAA Flow Control Conference, AIAA 2012-2952. doi: 10.2514/6.2012-2952.

[15] Wen X, Liu Y (2018) Lagrangian analysis of sweeping jets measured by time-resolved particle image velocimetry. *Experimental Thermal & Fluid Science*, vol. 97, pp 192-204. doi: 10.1016/j.expthermflusci.2018.04.014.

[16] Kara K, Kim D, Morris P J (2018) Flow separation control using sweeping jet actuator. *AIAA Journal*, vol. 56, pp 4604-4613. doi: 10.2514/1.J056715.

[17] Bons J, Benton S, Bernardini C, Bloxham M (2018) Active flow control for low-pressure turbines. *AIAA Journal*, vol. 56, pp 2687-2698. doi: 10.2514/1.J056697.

[18] Kiesner M, King R (2017) Multivariable closed-loop active flow control of a compressor stator cascade. *AIAA Journal*, vol. 55, pp 3371-3380. doi: 10.2514/1.J055728.

[19] Cooney J A, Szlatenyi C S, Fine N E (2016) The development and demonstration of a plasma flow control system on a 20 kW wind turbine. In: Proceedings of the 54th AIAA Aerospace Sciences Meeting, AIAA 2016-1302. doi: 10.2514/6.2016-1302.

[20] Taylor K, Leong C M, Amitay M (2015) Load control on a dynamically pitching finite span wind turbine blade using synthetic jets. *Wind Energy*, vol. 18, pp 1759-1775. doi: 10.1002/we.1789.

[21] Tran, S.A., Sahni, O., Corson, D., 2014. Synthetic jet based active flow control of dynamic stall phenomenon on wind turbines under yaw misalignment. AIAA 2014-0871. doi: 10.2514/6.2014-0871

[22] Rice T, Taylor K, Amitay M (2018) Wind tunnel quantification of dynamic stall on an S817 airfoil and its control using synthetic jet actuators. *Wind Energy*, vol. 22, pp 21-33. doi: 10.1002/we.2266.

[23] Rice T, Taylor K, Amitay M (2018) Quantification of the S817 airfoil aerodynamic properties and their control using synthetic jet actuators. *Wind Energy*, vol. 21, pp 823-836. doi: 10.1002/we.2197.

[24] Martin P, Wilson J, Berry J, Wong T C, Moulton M, McVeigh M (2008) Passive control of compressible dynamic stall. In: Proceedings of the 26th AIAA Applied Aerodynamics Conference, AIAA 2008-7506. doi: 10.2514/6.2008-7506.

[25] Mai H, Dietz G, Geissler W, Richter K, Bosbach J, Richard H, De Groot K (2008) Dynamic stall control by leading-edge vortex generators. *Journal of the American Helicopter Society*, vol. 53, pp 26-36. doi: 10.4050/JAHS.53.26.

[26] Xu H Y, Qiao C L, Ye Z Y (2016) Dynamic stall control on the wind turbine airfoil via a co-flow jet. *Energies*, vol. 9, pp 429. doi: 10.3390/en9060429.

[27] Leishman J G (1996) Seed particle dynamics in tip vortex flows. *Journal of Aircraft*, vol. 33, pp 823-825. doi: 10.2514/3.47020.

[28] Matsunuma T, Tsutsui Y (2002) LDV measurements of unsteady flow in a turbine rotor. In: Proceedings of the 32nd AIAA Fluid Dynamics Conference and Exhibit, AIAA 2002-2742. doi: 10.2514/6.2002-2742.

[29] Maeda T, Kamada Y, Murata J, Suzuki D, Kaga N, Kasigaki Y (2014) LDV measurements of boundary layer on rotating blade surface in wind tunnel. *Journal of Physics Conference Series*, vol. 555, 012057. doi: 10.1088/1742-6596/555/1/012057.

[30] Ning Z, Yang Z (2013) An experimental investigation on the control of tip vortices from wind turbine blade. In: Proceedings of the 51st AIAA Aerospace Sciences Meeting, AIAA 2013-1104. doi: 10.2514/6.2013-1104

[31] Ramasamy M, Leishman J G (2007) Benchmarking particle image velocimetry with laser Doppler velocimetry for rotor wake measurements. *AIAA Journal*, vol. 45, pp 2622-2633. doi: 10.2514/1.28130.

[32] Leishman J G, Coyne A J, Han Y O (1997) Measurements of the velocity and turbulence structure of a rotor tip vortex. *AIAA Journal*, vol. 35, pp 477-485. doi: 10.2514/2.120.

[33] Duraisamy K, Ramasamy M, Baeder J D, Leishman J G (2007) High resolution computational and experimental study of rotary-wing tip vortex formation. *AIAA Journal*, vol. 45, pp 2593-2602. doi: 10.2514/1.26575.

[34] Somers D M (1997) Design and experimental results for the S809 airfoil. National Renewable Energy Laboratory, NREL/SR-440-6918.

[35] Maldonado V, Boucher M, Ostman R, Amitay M (2010) Active vibration control of a wind turbine blade using synthetic jets. *International Journal of Flow Control*, vol. 1, pp 227-237. doi: 10.1260/1756-8250.1.4.227.

[36] Maldonado V, Farnsworth J, Gressick W, Amitay M (2010) Active control of flow separation and structural vibrations of wind turbine blades. *Wind Energy*, vol. 13, pp 221-237. doi: 10.1002/we.336.

[37] Cheeseman I C, Bennet W E (1955) The effect of the ground on a helicopter rotor in forward flight. Aeronautical Research Council, Reports & Memoranda 3021.

[38] Maldonado V, Gupta S (2017) Active flow control of a low reynolds number S809 wind turbine blade model under dynamic pitching maneuvers. *Open Journal of Fluid Dynamics*, vol. 7, pp 178-193. doi: 10.4236/ojfd.2017.72012.

[39] Amitay M, Glezer A (2018) Aerodynamic flow control using synthetic jet actuators. In: Koumoutsakos P, Mezic I (eds) Control of fluid flow. Springer Nature, Switzerland, pp 45-73.

[40] Leishman J G (2000) Principles of helicopter aerodynamics. Cambridge University Press, New York.

[41] Iversen J D (1976) Correlation of turbulent trailing vortex decay data. *Journal of Aircraft*, vol. 13, pp 338-342. doi: 10.2514/3.44529.